Robotica (2014) volume 32, pp. 245–256. © Cambridge University Press 2013
doi:10.1017/S0263574713001008

Tension distribution shaping via reconfigurable attachment in planar mobile cable robots

Xiaobo Zhou*, Seung-kook Jun and Venkat Krovi

Department of Mechanical and Aerospace Engineering, State University of New York at Buffalo, Buffalo, NY 14260, USA

(Accepted October 28, 2013. First published online: November 27, 2013)

SUMMARY
Traditional cable robots derive their manipulation capabilities using spooling winches at fixed base locations. In our previous work, we examined enhancing manipulation capabilities of cable robots by the addition of base mobility to spooling winches (allowing a group of mobile robots to cooperatively manipulate a payload using cables). Base mobility facilitated the regulation of the tension-direction (via active coordination of mobile bases) and allowed for better conditioning of the wrench-feasible workspace. In this paper we explore putting idler pulleys on the payload attachment as alternate means to simplify the design and enable practical deployment. We examine analysis of the system using ellipse geometry and develop a virtual cable-subsystem formulation (which also facilitates subsumption into the previously developed mobile cable robot analysis framework). We also seek improvement of the tension distribution by utilizing configuration space redundancy to shape the tension null space. This tension distribution shaping is implemented in the form of a tension factor optimization problem over the workspace and explored via both simulation and experimental studies.

KEYWORDS: Cable robots; Multi-robot systems; Design; Parallel manipulators; Redundant manipulators

1. Introduction

Cable robots have gained immense popularity in the past decades in bringing together benefits such as high payload capacity, significant workspace, low inertia, high energy efficiency, and ease of construction. Most of the past conventional cable robot research efforts, however, focused mainly on two major classes: (i) conventional cable robots with winches fixed in the inertial frame;[1–6] and (ii) towing robots with fixed-length cables on mobile bases,[7,8] with one notable exception of Donald et al.[9]

In our previous work,[10,11] we examined the enhancement of manipulation capabilities of cable robots by addition of base mobility (sliders, mobile platforms) to the spooling winches. Multiple individual mobile cable robot platforms could now attach themselves to a common payload and cooperatively manipulate the composite system. The characteristic feature was the reconfigurability and redundancy both within the individual mobile cable robot subchains and the composite system.

For example, one immediate benefit of the addition of redundancy was the ability to change tension direction. Cable robots can sustain only tension along the length of the cable, which can be quite limiting, especially when one seeks to achieve a large wrench-feasible workspace.[12] Multiple methods for altering and regulating the tension direction are illustrated in Fig. 1. For example, in case (a), attaching two cables to the same payload attachment point creates an analog to the "friction cone" in grasping – the effective tension direction can be anywhere within the cone spanned by the two cables; case (b) is similar to case (a) but is applicable to the towing scenario with fixed cable length and mobile bases; case (c) merges the capabilities of cases (a) and (b) by coordinating mobile bases and cable-control winches. In our previous paper,[10] we examined taking advantage of base mobility to achieve better control of the tension direction by actively repositioning of mobile bases.

* Corresponding author. E-mail: xzhou9@buffalo.edu

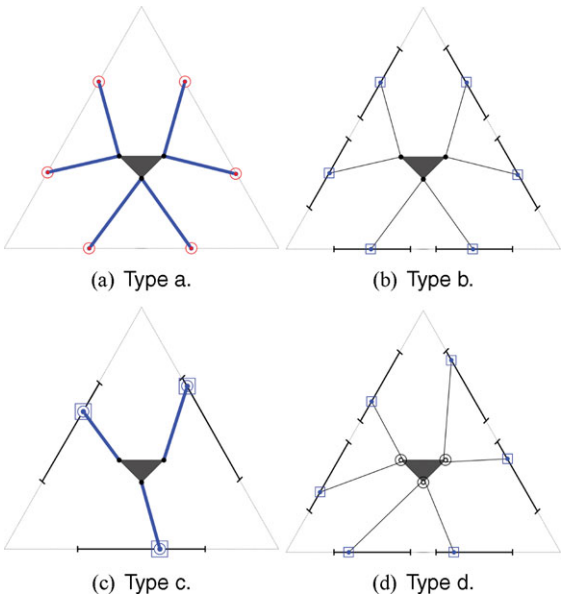

Fig. 1. (Colour online) Illustration of four case scenarios for tension-direction regulation: concentric circle with solid dots = active pulleys (winches), two concentric circles = passive/idler pulleys, black dots = fixed pins, squares with solid dots = pins on sliders, concentric circle with solid dots inside squares = winches on sliders, thick blue lines = variable-length cables, thin black lines = fixed-length cables.

In this paper we explore other ways to achieve regulation of the tension direction, specifically with modifications on the attachment modality to the common payload. Specifically, as shown in Fig. 1(d), we explore the use of passive/idler pulleys at the attachment point (in lieu of conventional pinned attachments). This allows distribution of the tension evenly at both sides, which creates an effective tension direction along the bisector.

One important motivation of such a design is to further simplify cable systems by eliminating the use of winches, which tend to be relatively complicated to design/control and tend to contribute to cable length estimation errors. We note that there are design approaches that had explored alternative locations of pulley blocks[13] in order to optimize local performance index of planar cable robots (with point mass end-effectors). There is also some recent work[14,15] on use of closed-loop cable transmissions with idler pulleys to serve as timing belts. Other examples of usage of closed-loop cable transmissions may be seen in the CableCam system,[16] but is presented without supporting analysis.

Challenges arise due to the requirement to control the cable length to maintain tension. Merlet and Daney[17] presented a new design for cable robot that uses linear actuator with a set of pulleys to amplify the change of cable length without using winches. Our proposed solution merges the benefits of the above: It employs fixed-length cables combined with idler pulleys to achieve change in the effective cable length joining the base to the moving platform.

Three potential solutions are illustrated in Fig. 2. For example, in Fig. 2(a), the cable is routed through the passive-pulley on payload with one end fixed to the ground, the other end spooled by an active-pulley (winch). This winch/fixed configuration has the potential benefit of simplicity of control but cannot help independent realization of cable length and tension. Figure 2(b) illustrates a more general two-winch case, connected by a variable-length cable routed through a passive pulley on the payload. The winches can potentially be coordinated to allow independent control of cable-length and cable-tension magnitudes. However, they offer limited ability to control the direction of the cable tension (that we believe is far more critical).

Instead, in this paper, we will focus on the staged introduction of reconfigurability via the double-slider case, fixed cable length case, shown in Fig. 2(c). Herein, the two ends of a fixed-length cable are attached to the sliders, and the cable is routed through the passive pulley on the payload. Note that, while the mobile bases are considered to be sliders here, this analysis can be readily extended to encompass other forms of base mobility.

https://doi.org/10.1017/S0263574713001008 Published online by Cambridge University Press

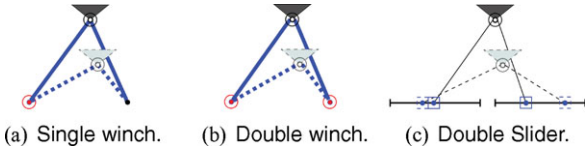

Fig. 2. (Colour online) Illustration of different pulley types (solid and dashed lines represent two configurations).

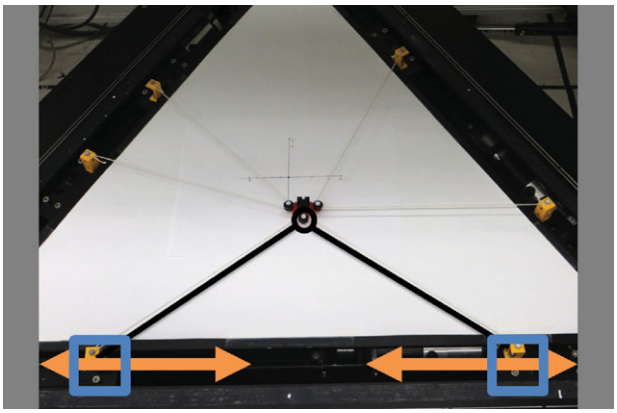

Fig. 3. (Colour online) Experimental setup implementing the type d system (shown in Fig. 1(d)) with one side subsystem marked up.

The advantages of this setup are: (i) even distribution of load (i.e., if friction is ignored in the pulley, tensions are equal on both sides yielding "mechanically averaging" of the tension distribution); (ii) allowing distributed coordination control with relative change of position (as opposed to traditional towing case where tow-robots can come no closer than the fixed tow-cable radius); (iii) allowing decoupling cable-length and cable-tension control that traditionally limits winched systems; (iv) simplicity of construction with the elimination of winch-introduced cable-length errors by virtue of direct cable connection to sliders. One potential disadvantage is the limited workspace that arises when the cable lengths are fixed. However, the workspace limit does not pose a problem if the bases are not constrained by the slider limits (or are full-fledged mobile bases capable of freely moving in the entire space). Additionally, the workspace can be greatly extended by allowing the cable length to vary as well, which we propose to examine in the future.

The paper is organized as follows: Section 2 focuses on the formulation of the kinematics of the physical double-slider, fixed cable length case with the development of an equivalent simplified kinematic virtual-subsystem (and mappings between the two). Section 3 examines the exploitation of significant redundancy to assist in the tension null space shaping and controlling the tension factor for a planar implementation. Section 4 presents the experimental implementation of the above framework to help perform desired physical interaction tasks with the environment (in the presence of uncertainty and disturbances). Specifically, we present results of tracing the letter R with end-effector-mounted pen (with an OptiTrack motion-capture system providing the ground-truth). Finally, we conclude with a discussion of the performance of the quasi-static tension-regulation framework presented here and avenues for the future work.

2. Formulation

Figure 3 depicts the composite system wherein a triangular end-effector is controlled by three sets of double-sliders that can reciprocate along the side of an equilateral base triangle. Each set of double-slider is attached to the ends of a fixed cable length, routed around a passive-pulley attached to a corner of the end-effector. The individual sliders need to be controlled so as to maintain tension in the fixed-length cable. These coordination requirements can be described by the governing geometric equations of an ellipse (see Fig. 4). The two sliders (F_1, F_2) serve as foci, the fixed length of cable ($F_1 P F_2$) $L = 2a$, where a is the semi-major axis length.

https://doi.org/10.1017/S0263574713001008 Published online by Cambridge University Press

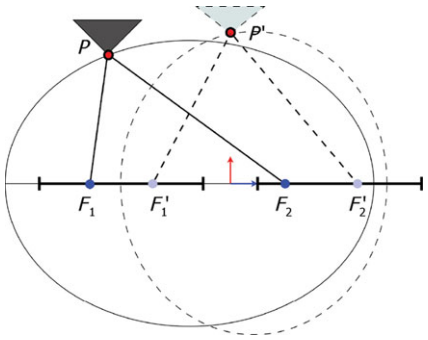

Fig. 4. (Colour online) Illustration of feasible idler pulley (P) locations on ellipses (solid and dashed) formed by different slider (F_1, F_2) positions.

2.1. *The original system*

We first illustrate the forward kinematics, inverse kinematics, and workspace of the system, utilizing the geometry of ellipse. Subsequently, we introduce the notion of an equivalent virtual cable subsystem (that replaces this physical subsystem for analysis purposes).

2.1.1. Forward and inverse kinematics. By equating the three ellipse equations (see (1), also referring to Fig. 4) and enforcing the idler pulleys $P_i(x_{pi}, y_{pi})$ to lie on the ellipses, we can solve for the payload pose (x_e, y_e, ϕ_e) from left $F_{1i}(x_{1i}, y_{1i})$ and right $F_{2i}(x_{2i}, y_{2i})$ slider positions, i.e., the forward kinematics.

$$\frac{(x_{pi} - x_{oi})^2}{a_i^2} + \frac{(y_{pi} - y_{oi})^2}{b_i^2} = 1, \quad \forall i \in \{1, 2, 3\}, \tag{1}$$

where $x_{oi} = (x_{1i} + x_{2i})/2,\ y_{oi} = (y_{1i} + y_{2i})/2, a_i = a = L/2,\ c_i = (x_{2i} - x_{1i})/2,\ b_i = \sqrt{a_i^2 - c_i^2}$. Then from the three idler pulley locations we can easily determine the payload pose. While analytic solutions are feasible, they tend to be difficult to obtain. Hence, for the purpose of this paper we will rely on the numerical solution alone.

Similarly we can also calculate the slider position from payload position, i.e., the inverse kinematics, based on the geometry of the ellipse, shown in Fig. 6(a),

$$\begin{aligned} x_{1i} &= x_{oi} - c_i \\ x_{2i} &= x_{oi} + c_i \end{aligned}, \tag{2}$$

where $x_{oi} = x_{pi} + \frac{a_i^2}{b_i^2} k y_{pi},\ c_i = \sqrt{a_i^2 - b_i^2}$, and k is the slope of the tangent to the ellipse at the idler pulley position, which is determined by the payload pose.

2.1.2. Kinematic workspace. All feasible trajectories of the three idler pulleys (vertices of the end-effector triangle) lie on the classes of ellipses formed by varying the locations of the foci (shown in Fig. 5(a)). A sample numerical evaluation of the constant orientation workspace at $\phi_e = 0^\circ$ verifies the shape of the kinematic workspace as shown in Fig. 5(b). This serves only as an initial starting point for feasible workspace analysis. Careful treatment of wrench-closure[18] needs to be determined for usable cable robots, as we do in Section 3.

2.2. *Equivalent virtual subsystem*

We seek to cast this problem into our earlier developed mobile cable robots framework for a couple of reasons: (i) Problem formulation may not be as trivial in more complicated spatial cases; and (ii) we desire the analysis to be more generally applicable.

The tensions in the cable are the same on both sides of the passive pulleys at the vertex of the end-effector (assumed to be frictionless). Then the effective tension direction PN is always along the bisector of the angle $\angle F_1 P F_2$. Ellipse geometry also dictates that PN is normal at point P on

https://doi.org/10.1017/S0263574713001008 Published online by Cambridge University Press

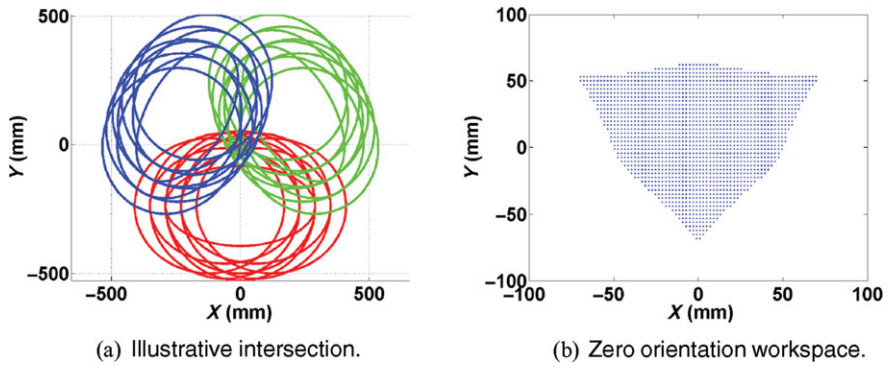

(a) Illustrative intersection. (b) Zero orientation workspace.

Fig. 5. (Colour online) Numerical evaluation of the kinematic workspace of the experimental setup.

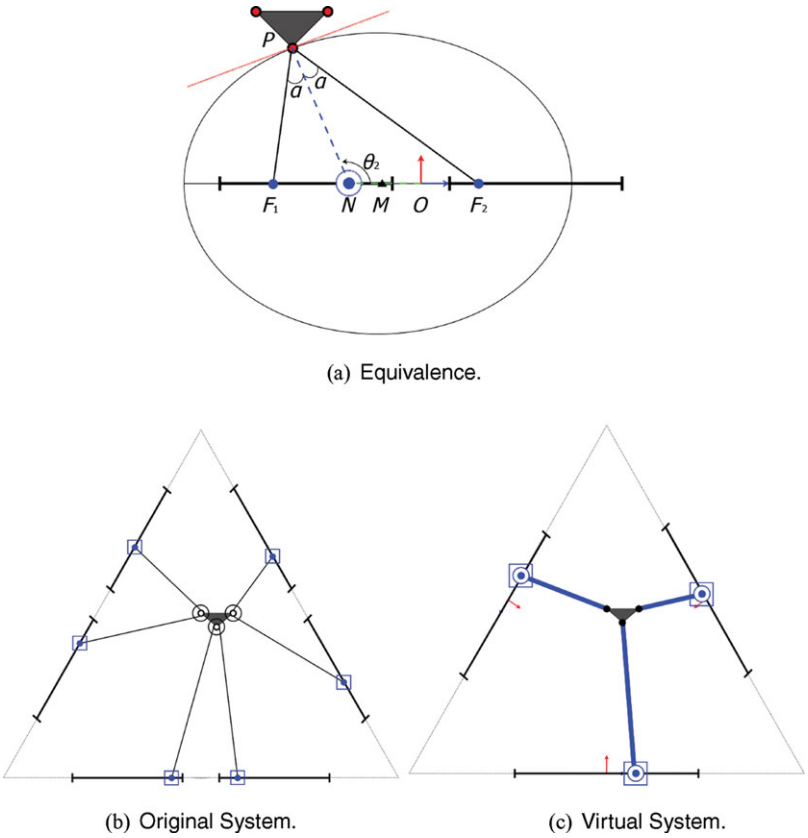

(a) Equivalence.

(b) Original System. (c) Virtual System.

Fig. 6. (Colour online) Illustration of (b) original, and (c) equivalent virtual systems that exploit the equivalence depicted.

the ellipse, perpendicular to the tangent. Therefore, we can create an equivalent virtual subsystem for each pair of sliders, which corresponds to our previous model of mobile cable robots.[10]

This can be seen from Fig. 6(a). If we replace the two-slider cable-pulley system F_1PF_2 with the slider-winch cable virtual subsystem ONP (shown in dashed green), then we end up with the same model with variable mappings $ON = l_1$, $\angle MNP = \theta_2$, and $NP = l_3$. M is the middle point between F_1 and F_2, i.e., center of the ellipse, O is the middle point of the two sliders (subscript $_i$ indicating the number of subsystem have been dropped for notation simplicity).

In order to be able to use our previous analysis framework, we show the mapping between virtual and real subsystems (dropping the subscript $_i$) to allow for conversion back and forth.

https://doi.org/10.1017/S0263574713001008 Published online by Cambridge University Press

2.2.1. Forward mapping. Referring to Fig. 6(a), the forward mapping, i.e., calculating the equivalent virtual subsystem configuration from the known real subsystem slider positions, can be obtained as

$$\begin{aligned} l_1 &= e^2(x_p - x_o) + x_o, \\ \theta_2 &= \arctan 2(y_p, x_p - l_1) \\ l_3 &= \sqrt{(x_p - l_1)^2 + y_p^2}, \end{aligned} \tag{3}$$

where $e = c/a$ is the eccentricity of the ellipse.

2.2.2. Inverse mapping. Once we find the configuration of the virtual subsystem (i.e., $ON = l_1, \angle ONP = \theta_2, NP = l_3$), we can also map it back to the real structure (i.e., calculate $x_o = OM$, $x_1 = OF_1$, $x_2 = OF_2$) for control. Since F_1 and F_2 are the foci of the ellipse, PN is the normal perpendicular to the tangent at P. The inverse mapping is obtained by first calculating the idler pulley position P from the virtual subsystem, then using the inverse kinematics as shown in Section 2.1.1.

2.3. Formulation for equivalent system

The formulation of the equivalent virtual system falls into the framework we have presented in Zhou *et al.*,[11] which we briefly outline here. Referring to Fig. 6(c), we first find the body twists in each successive joint frame:

$$\underset{\sim}{t}^b_{01_i} = \begin{bmatrix} \dot{l}_{1_i} \\ 0 \\ 0 \end{bmatrix}, \quad \underset{\sim}{t}^b_{12_i} = \begin{bmatrix} 0 \\ 0 \\ \dot{\theta}_{2_i} \end{bmatrix}, \quad \underset{\sim}{t}^b_{23_i} = \begin{bmatrix} \dot{l}_{3_i} \\ 0 \\ 0 \end{bmatrix}. \tag{4}$$

Then compose the spatial Jacobian for each virtual subsystem:

$$J^s_{Wvi} = \begin{bmatrix} \cos\phi_{0i} & y_{0i} + l_{1i}\sin\phi_{0i} & \cos(\phi_{0i} + \theta_{2i}) \\ \sin\phi_{0i} & -x_{0i} - \cos\phi_{0i} l_{1i} & \sin(\phi_{0i} + \theta_{2i}) \\ 0 & 1 & 0 \end{bmatrix}, \tag{5}$$

where $(x_{0i},\ y_{0i},\ \phi_{0i})$ is the pose of the center of sliders frame $\{O_i\}$ in world fixed frame $\{W\}$. The cable wrench can be expressed in the payload frame $\{e\}$ via co-adjoint transformation as follows:

$${}^e\underset{\sim}{w}_i = P_{ei} f_i = \begin{bmatrix} -\cos\gamma_i \\ \sin\gamma_i \\ y_{ep_i}\cos\gamma_i + x_{ep_i}\sin\gamma_i \end{bmatrix} f_i \ . \tag{6}$$

Then we find the map and constraint (7)

$$\begin{aligned} P_e \mathbf{f} &= \underset{\sim}{w} \\ J_T \dot{\mathbf{q}} &= P_e^T \dot{\mathbf{x}}_e \end{aligned}, \tag{7}$$

where

$$J_T = \begin{bmatrix} J_{t1} & \mathbf{0} & \mathbf{0} \\ \mathbf{0} & J_{t2} & \mathbf{0} \\ \mathbf{0} & \mathbf{0} & J_{t3} \end{bmatrix}, \quad P_e^T = \begin{bmatrix} P_{e1}^T \\ P_{e2}^T \\ P_{e3}^T \end{bmatrix}, \quad \mathbf{f} = \begin{bmatrix} f_1 \\ f_2 \\ f_3 \end{bmatrix}, \tag{8}$$

and $J_{ti} = B_{p_i}^T Ad^{-1}_{g_{wp_i}} J^s_{Wv_i} = [-\cos\theta_{2_i},\ \cos(\phi_{0_i} + \theta_{2_i})y_e + \sin(\phi_{0_i} + \theta_{2_i})(x_{0_i} + \cos\phi_{0_i} l_{1_i}) - \cos(\phi_{0_i} + \theta_{2_i})(y_{0_i} + l_{1_i}\sin\phi_{0_i}) - \sin(\phi_{0_i} + \theta_{2_i})x_e + y_{p_i}\cos\gamma_i + x_{p_i}\sin\gamma_i, -1]$, where $\gamma_i = \phi_e - \phi_{0i} - \theta_{2i}$, f_i is the tension in each cable, $\mathbf{q} = [l_{1_1}, \theta_{2_1}, l_{3_1}, l_{1_2}, \theta_{2_2}, l_{3_2}, l_{1_3}, \theta_{2_3}, l_{3_3}]^T$ are the

https://doi.org/10.1017/S0263574713001008 Published online by Cambridge University Press

configuration variables of the equivalent virtual system, $\mathbf{x}_e = [x_e, y_e, \phi_e]^T$ is the payload pose, and $\underset{\sim}{w} = [F_x, F_y, M_z]^T$ is the external wrench.

Since we only have three effective cables, the controllable external wrench is only two-dimensional (2D) (F_x, F_y). Therefore, the effective pulling map is

$$P = \begin{bmatrix} -\cos\gamma_1 & -\cos\gamma_2 & -\cos\gamma_3 \\ \sin\gamma_1 & \sin\gamma_2 & \sin\gamma_3 \end{bmatrix}. \tag{9}$$

Although due to physical construction we have a rigid body payload, its dimension is small enough that we just consider it as point mass and ignore its orientation and the corresponding moment about the vertical axis.

3. Tension Analysis

There have been several works in the literature that deal with tension analysis for completely restrained cable robots.[18–22] In this paper we will focus our discussion on the analysis and optimization of the tension factor TF, which is defined by[23]

$$TF = \frac{\min(\mathbf{f})}{\max(\mathbf{f})}. \tag{10}$$

Specifically, we introduce the concept of tension null space shaping utilizing the redundancy in our system for achieving equal tension distribution.

3.1. Conventional cable robots

In conventional cable robots (i.e., Fig. 1(a)), the redundancy is only in the tension magnitudes. The optimization problem entails determination of the applied tension in each cable to generate/resist external wrenches while keeping internal antagonistic forces low (i.e., small homogeneous solution).

If there is only one redundant cable $(n + 1)$, then the tension null space is only 1D, the TF is therefore fixed. With more redundant cables $(n + k)$, the homogeneous solution is then a linear combination of the null space basis N_i, i.e.,

$$F_h = \sum_{i=1}^{k} c_i N_i, \quad (k > 1). \tag{11}$$

Then it is possible to minimize TF by determining the unknown c_is (which can be solved as a linear programming problem in $O(n)$ time).

3.2. Tension null space shaping by configuration null space repositioning

However, in our setup, in the case of only one redundant cable, due to the configuration space redundancy, we have the ability to change the directions of tensions, therefore allowing a structural reconfiguration for optimal tension distribution by shaping the tension null space.

In the conventional case, the tension factor is solely a function of tension magnitudes, i.e., $TF(\mathbf{f})$. The major difference herein is that the tension factor is also a function of configuration, i.e., $TF(\mathbf{q}, \mathbf{f})$, where $\mathbf{f}$ and $\mathbf{q}$ are the cable tension and joint configuration variable vectors respectively. Hence, a linear programming approach proves inadequate since the problem is nonlinear.

The kinematic redundancy is illustrated in Fig. 7. There are lots of feasible slider configurations that yield the same pulley position. As can be seen, the effective tension direction is also the direction of the virtual cable subsystem. Such kind of reconfiguration changes the pulling map P, and the tension null space can therefore be shaped.

For our setup, we can compute the null space to be

$$N_v = \text{Null}(P) = \begin{bmatrix} \sin(\theta_{2_2} - \theta_{2_3} + \phi_{0_2} - \phi_{0_3}) \\ \sin(\theta_{2_3} - \theta_{2_1} + \phi_{0_3} - \phi_{0_1}) \\ \sin(\theta_{2_1} - \theta_{2_2} + \phi_{0_1} - \phi_{0_2}) \end{bmatrix}. \tag{12}$$

https://doi.org/10.1017/S0263574713001008 Published online by Cambridge University Press

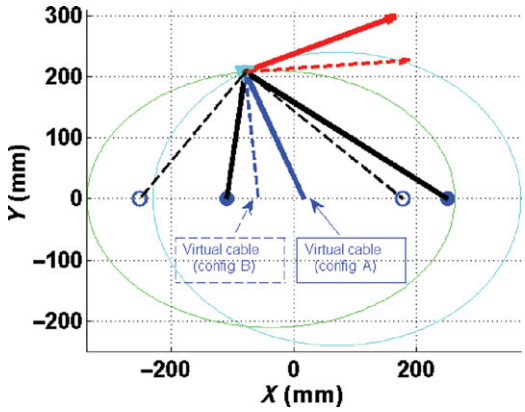

Fig. 7. (Colour online) Illustration of kinematic redundancy (for a fixed pulley position, the solid lines correspond to one feasible configuration A, while the dashed lines correspond to configuration B, black line = fixed-length cable, blue line = virtual cable, red line with arrow = tangent to ellipse).

For this specific configuration, $\phi_{0_2} - \phi_{0_3} = \phi_{0_3} - \phi_{0_1} = \phi_{0_1} - \phi_{0_2} = 120^\circ$ we see that we get the optimal (i.e., maximum TF) when $\theta_{2_1} = \theta_{2_2} = \theta_{2_3}$. Intuitively, the three virtual cables split the plane equally at 120° relative angles between each other. So the optimal configuration is obtained (we note it has multiple optima as only relative angles matter, but we can fix one angle to be say $\theta_{2_1} = \pi/2$, then the rest are the same). In fact, this is a good configuration because these angles result in the yaw moment to be almost zero since the lines intersect at a point which is very close to the geometric center of the payload. Therefore, the payload is able to maintain almost zero orientation throughout trajectory. For more general 3D cases, the optimum may not be as trivial and will require careful nonlinear optimization.

Although N_v determines the tension distribution in the equivalent virtual system, it does not reflect the true tension distribution in the real system. Referring to Fig. 6(a), we see $f_{PF_1} = f_{PF_2}$ and $f_{PN} = 2 f_{PF_1} \cos\alpha$. Therefore, for the real system to have equal tension distribution, we have to weight N_v by

$$W = \begin{bmatrix} 1/\cos\alpha_1 & 0 & 0 \\ 0 & 1/\cos\alpha_2 & 0 \\ 0 & 0 & 1/\cos\alpha_3 \end{bmatrix}, \tag{13}$$

where α_i is the angle between the actual cable and virtual cable of each subsystem as shown in Fig. 6(a). Then $N_r = W N_v$ reflects the actual tension null vector direction. Obviously, the desired best possible null tension vector is $N_d = [1/\sqrt{3}, 1/\sqrt{3}, 1/\sqrt{3}]$, we can calculate the angle between the desired best direction N_d and the actual unit null vector N as a measure of quality of configuration. This measure can be used for optimizing configuration for non-trivial cases,

$$\delta = \arccos(N^T N_d). \tag{14}$$

In the presence of more cables, the redundancy resolution approach can be used to simultaneously (i) optimize wrench direction (in the sense of reconfiguring the base locations); and (ii) optimize tension through TF maximization as in the conventional case. We note, this is just one way of resolving the redundancy, using tension factor as the objective. Other pertinent performance measures based on the stiffness matrix (or its subcomponents, i.e., Yu *et al.*[24]) can be used as well. We also note that other authors have explored the use of force index and dexterity as local performance measures for the optimal design of cable pulley block positions.[13]

https://doi.org/10.1017/S0263574713001008 Published online by Cambridge University Press

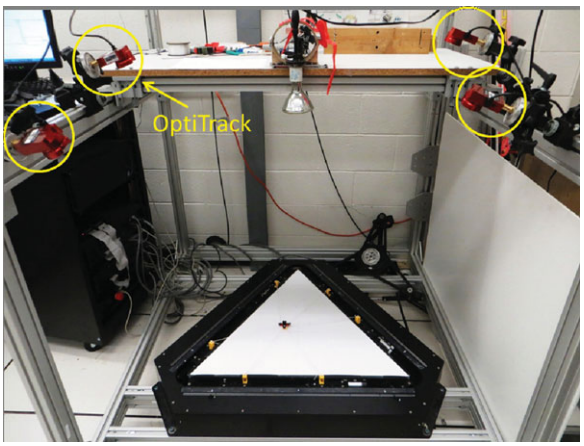

Fig. 8. (Colour online) Experimental setup with ground truth measurement via an OptiTrack system.

4. Experimental Results

4.1. Setup

As shown in Fig. 8, the experimental setup is based on using six linear sliders in the plane (two on each side of an equilateral triangle). Three cables are each routed through a pulley on the payload, with ends fixed on each of the two sliders on a given side of the triangle. The three sides form a right triangle, the distance from its geometric center to one side is 238 mm, the range of sliders are limited to [5, 245] mm, the three cable lengths are fixed to 580 mm, and the payload shape is $30 \times 15\sqrt{2} \times 15\sqrt{2}$ mm. We note in this setup, due to physical construction limitations, the payload is not an ideal point mass, but a rigid body having 3 degrees of freedom (DOF). With the effective cables being three, exact wrench closure is only possible for 2 DOF, we leave the yaw moment generally uncontrolled. However, since the payload dimension is small enough, this is not a big issue. Also, because we have the freedom of choosing the direction of effective tensions, we can make certain orientation control, as will be demonstrated in the experiment. The OptiTrack motion capture system is used for ground truth verification, reflective markers are placed on sliders and pulleys. At present, the control is in joint space (i.e., each slider with PD control), we are working on operational space dynamic control.

4.2. Null configuration space motion

In this case, we show the kinematic redundancy which can be used to shape the tension null space. As can be seen in Fig. 9, for the same end effector position, the second joint space configuration corresponds to the best possible TF, other configurations have lower TF.

We can also see that the TF for the virtual system is generally different from the real system. For configuration 1, $TF_v = 0.448 < TF_r = 0.496$, this is also evident from the quality measure $\delta_v = 0.298 > \delta_r = 0.267$, i.e., the "distance" between the virtual null vector and the desired null vector is larger than the "distance" between the real null vector and the desired null vector, i.e., the real system has better tension distribution than the virtual system. At configuration 3, the situation is opposite, $TF_v = 0.465 > TF_r = 0.406$, $\delta_v = 0.285 < \delta_r = 0.335$, i.e., the virtual system has better tension distribution than the real system. For configuration 2, $TF_v = 1 > TF_r = 0.926$, $\delta_v = 0 < \delta_r = 0.037$, i.e., the virtual null vector coincides with the desired null vector, which corresponds to ideal even tension distribution, while there is a small "distance" between the real null vector and the desired null vector. This means that ideal tension distribution of the virtual system does not guarantee ideal tension distribution of the real system, therefore requiring the weighting matrix to adjust for the actual tension in cables.

4.3. Letter writing example

As an illustration of the concept, we put a pen on the payload to write the letter "R" as shown in Fig. 10.

https://doi.org/10.1017/S0263574713001008 Published online by Cambridge University Press

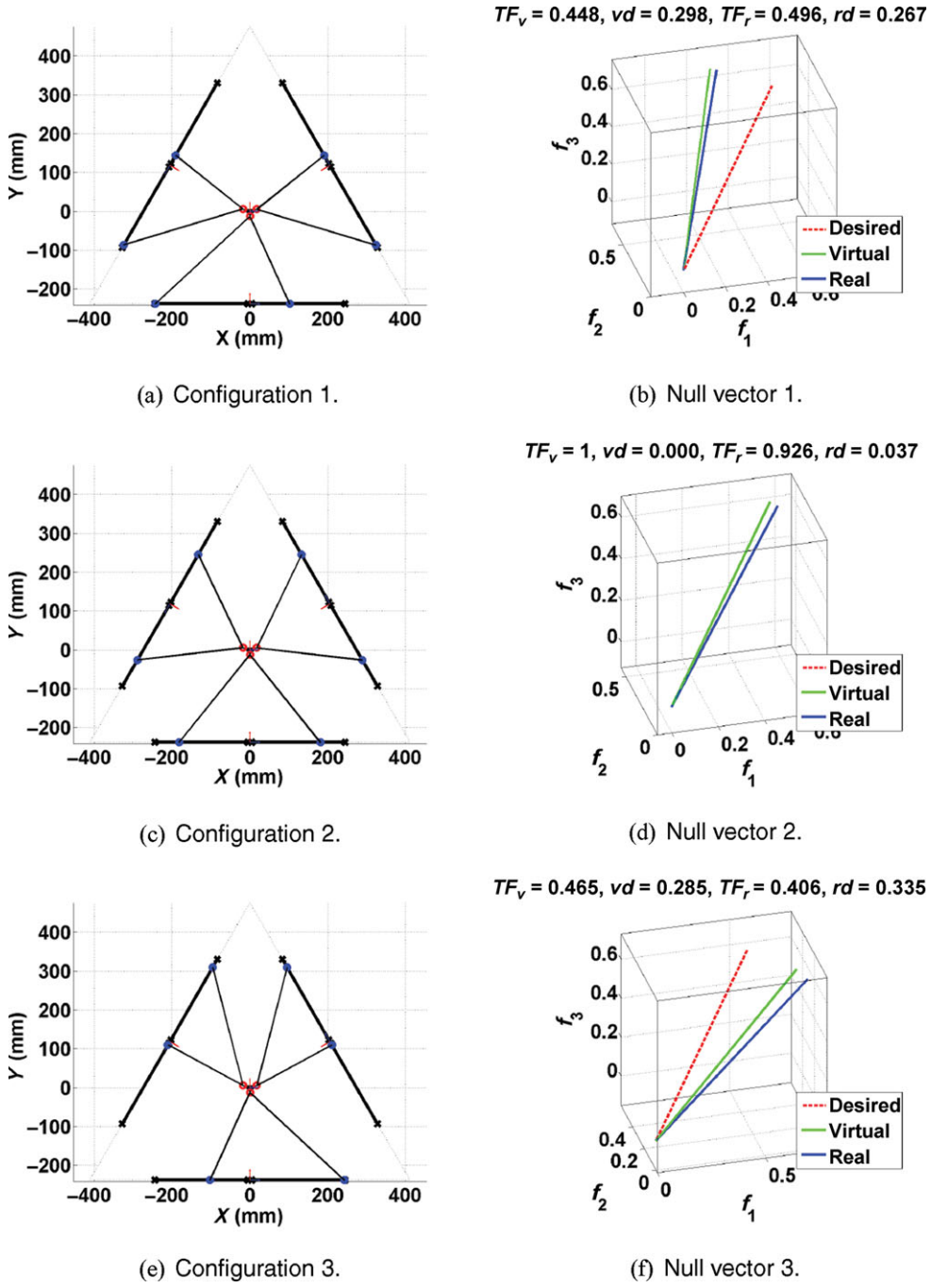

Fig. 9. (Colour online) Null configuration space motion corresponding to null tension space shape.

The desired trajectory is composed of one straight vertical line, followed by two horizontal parabolas. During the trajectory, it is set that $\theta_{2i} = \pi/2$ such that as discussed in Section 3.2, the orientation of the payload is maintained to be zero as much as possible. Otherwise uncontrolled yaw motion will cause large errors since the pen is not at the exact geometric center. The actual trajectory is captured by the motion tracking system. The result is shown in Fig. 11, and a video is available in Zhou *et al.*.[25]

We note here that we are just using quasi-static position control in joint space. We set the optimal configuration to have the best possible TF using kinematic redundancy. However, although we are not explicitly controlling tensions, we are able to trace the trajectory while accommodating certain amount of disturbance (in the case of pen tip friction, pen weight inertial oscillation, etc.).

https://doi.org/10.1017/S0263574713001008 Published online by Cambridge University Press

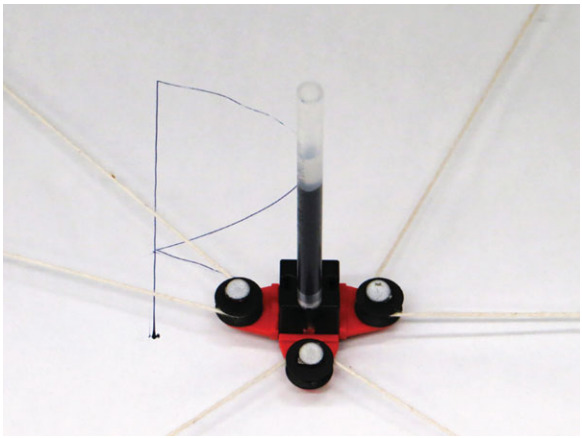

Fig. 10. (Colour online) Writing letter R.

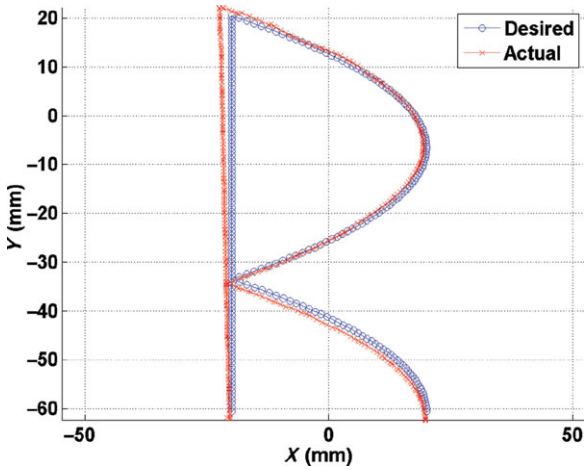

Fig. 11. (Colour online) Actual versus desired trajectory.

5. Discussion

In this paper, we explored alternate means for regulating both tension direction and magnitude by design modifications on the type/location of the cable attachment to the common payload, which leads to a new type of cooperating mobile cable robots. This new capability gives cable robots better tension control allowing for more uniform load distribution. We also showed that this type of cable robots can be analyzed within the mobile cable robot framework presented in our previous work.[10,11] We exploited the configuration space redundancy for shaping of tension null space via minimization of an appropriate null space measure over the workspace, yielding a more uniform tension distribution. While the case study presented here uses linear sliders as a proof of concept, practical usage applications will be put on full-fledged mobile platforms such as mobile robots. Work is ongoing to characterize the disturbance-rejection characteristics endowed by this new configuration. Further, the planar case results (both simulation and experimental) are being extended to the spatial case. Finally, we are enhancing the hardware to extend beyond the current quasi-static case, to encompass fully dynamic control with tension regulation.

Acknowledgments

This work was supported in part by the National Science Foundation Grants CNS-1135660 and IIS-1319084.

References

1. J. Albus, R. Bostelman and N. Dagalakis, "The NIST ROBOCRANE," *J. Robot. Syst.* **10**(5), 709–724 (1993).
2. S.-R. Oh and S. K. Agrawal, "Cable suspended planar robots with redundant cables: Controllers with positive tensions," *IEEE Trans. Robot.* **21**(3), 457–465 (2005).
3. J. V. Zitzewitz, G. Rauter, R. Steiner, A. Brunschweiler and R. Riener, "A Versatile Wire Robot Concept as a Haptic Interface for Sport Simulation," **In**: *Proceedings of the 2009 IEEE International Conference on Robotics and Automation (ICRA 2009)*, Kobe, Japan (2009) pp. 313–318.
4. M. Hiller, S. Fang, S. Mielczarek, R. Verhoeven and D. Franitza, "Design, analysis and realization of tendon-based parallel manipulators," *Mech. Mach. Theory* **40**(4), 429–445 (2005).
5. R. Nan, "Five hundred meter aperture spherical radio telescope (fast)," *Sci. China Ser. G* **49**(2), 129–148 (2006).
6. S. Perreault and C. M. Gosselin, "Cable-driven parallel mechanisms: Application to a locomotion interface," *J. Mech. Des.* **130**(10), 102301 (2008).
7. P. Cheng, J. Fink, V. Kumar and J.-S. Pang, "Cooperative towing with multiple robots," *ASME J. Mech. Robot.* **1**(1), 1–8 (Feb. 2009).
8. N. Michael, J. Fink and V. Kumar, "Cooperative manipulation and transportation with aerial robots," **In**: *Proceedings of Robotics: Science and Systems V*, Seattle, USA (online) (2009, June).
9. B. Donald, L. Gariepy and D. Rus, "Distributed Manipulation of Multiple Objects Using Ropes," **In**: *Proceedings of the 2000 IEEE International Conference on Robotics and Automation (ICRA 2000)*, San Francisco, CA, vol. 1 (2000) pp. 450–457.
10. X. Zhou, C. P. Tang and V. Krovi, "Analysis Framework for Cooperating Mobile Cable Robots," **In**: *Proceedings of the 2012 IEEE International Conference on Robotics and Automation (ICRA 2012)*, Karlsruhe, Germany (May 2012) pp. 3128–3133.
11. X. Zhou, C. Tang and V. Krovi, *Cooperating Mobile Cable Robots: Screw Theoretic Analysis*, Ser. Lecture Notes in Electrical Engineering, vol. 57 (Springer, Berlin, Germany, 2013), Ch. 7, pp. 109–123.
12. P. Bosscher, A. T. Riechel and I. Ebert-Uphoff, "Wrench-feasible workspace generation for cable-driven robots," *IEEE Trans. Robot.* **22**(5), 890–902 (Oct. 2006).
13. G. Rosati, D. Zanotto and S. K. Agrawal, "On the design of adaptive cable-driven systems," *J. Mech. Robot.* **3**(2), 021 004–021 004 (Mar. 2011).
14. H. Liu, C. Gosselin and T. Laliberte, "A Spatial Spring-Loaded Cable-Loop-Driven Parallel Mechanism," *International Design Engineering Technical Conferences and Computers and Information in Engineering Conference (ASME 2011)* (2011).
15. T. Laliberte, C. Gosselin and D. Gao, "Closed-Loop Transmission Routings for Cartesian Scara-Type Manipulators," *International Design Engineering Technical Conferences and Computers and Information in Engineering Conference (ASME 2010)* , Vancouver, British Columbia (2010).
16. J. Rodnunsky, "System and Method for Moving Objects Within Three-Dimensional Space," US Patent 6 809 495 (2004).
17. J.-P. Merlet and D. Daney, "A New Design for Wire-Driven Parallel Robot," *2nd World Congress on Design and Modelling of Mechanical Systems* (2007).
18. M. Gouttefarde and C. M. Gosselin, "Analysis of the wrench-closure workspace of planar parallel cable-driven mechanisms," *IEEE Trans. Robot.* **22**(3), 434–445 (Jun. 2006).
19. S.-R. Oh and S. K. Agrawal, "Cable suspended planar robots with redundant cables: controllers with positive tensions," *IEEE Trans. Robot.* **21**(3), 457–465 (2005).
20. M. Gouttefarde, J. P. Merlet and D. Daney, "Wrench-Feasible Workspace of Parallel Cable-Driven Mechanisms," **In**: *Proceedings of the 2007 IEEE International Conference on Robotics and Automation (ICRA 2007)*, Roma, Italy (2007) pp. 1492–1497.
21. L. Mikelsons, T. Bruckmann, M. Hiller and D. Schramm, "A Real-Time Capable Force Calculation Algorithm for Redundant Tendon-Based Parallel Manipulators," **In**: *Proceedings of the 2008 IEEE International Conference on Robotics and Automation (ICRA 2008)*, Pasadena, CA (2008) pp. 3869–3874.
22. P. Borgstrom, B. Jordan, G. Sukhatme, M. Batalin and W. Kaiser, "Rapid computation of optimally safe tension distributions for parallel cable-driven robots," *IEEE Trans. Robot.* **25**(6) 1271–1281 (2009).
23. C. B. Pham, S. H. Yeo, G. Yang and I. M. Chen, "Workspace analysis of fully restrained cable-driven manipulators," *Robot. Auton. Syst.* **57**(9), 901–912 (2009).
24. K. Yu, L.-F. Lee, C. P. Tang and V. Krovi, "Enhanced trajectory tracking control with active lower bounded stiffness control for cable robot," **In**: *Proceedings of the 2010 IEEE International Conference on Robotics and Automation (ICRA 2010)*, Anchorage, AK (May 2010) pp. 669 –674.
25. X. Zhou, S.-K. Jun and V. Krovi, "Video-mobile cable robot with wrench reconfigurability." (Online). Available at: http://youtu.be/lMkL6diA32I (accessed July 9, 2013).

https://doi.org/10.1017/S0263574713001008 Published online by Cambridge University Press